Open

Light: Science & Applications (2013) 2, e90; doi:10.1038/lsa.2013.46
© 2013 CIOMP. All rights reserved 2047-7538/13
www.nature.com/lsa

ORIGINAL ARTICLE

Light spectral filtering based on spatial adiabatic passage

Ricard Menchon-Enrich[1], Andreu Llobera[2], Jordi Vila-Planas[2], Víctor J Cadarso[3], Jordi Mompart[1] and Veronica Ahufinger[1]

We present the first experimental realization of a light spectral filter based on the spatial adiabatic passage technique. We demonstrate that a fully integrable CMOS-compatible system of three coupled identical total internal reflection silicon oxide waveguides with variable separation along their propagation direction can be used simultaneously as a low- and high-pass spectral filter within the visible range of wavelengths. Light is injected into the right waveguide, and after propagating along the system, long wavelengths are transferred into the left output, whereas short wavelengths propagate to the right and central outputs. The stopband reaches values up to −11 dB for the left output and approximately −20 dB for the right plus central outputs. The passband values are close to 0 dB for both cases. We also demonstrate that the filtering characteristics of the device can be controlled by modifying the parameter values, which define the geometry of the triple-waveguide system. However, the general filtering behavior of the system does not critically depend on technological variations. Thus, the spatial adiabatic passage filtering approach constitutes an alternative to other integrated filtering devices, such as interference or absorbance-based filters.

Light: Science & Applications (2013) **2,** e90; doi:10.1038/lsa.2013.46; published online 16 August 2013

Keywords: CMOS-compatible technology; integrated optics devices; spatial adiabatic passage; wavelength filtering devices

INTRODUCTION

Photonic integrated circuits (PICs) have the potential to revolutionize computing platforms due to the high speed and quality of light-based communications. Recently, photonic integration has been pushed forward by taking advantage of complementary metal-oxide-semiconductor (CMOS)-compatible technology, which allows high quality PICs to be obtained with high-index contrasts.[1,2] Due to this contrast, sharp bends can be implemented, leading to significant miniaturization of the optical components. Furthermore, CMOS-compatibility allows the usage of already developed mass-production fabrication techniques for electronic components on the one hand and the monolithic integration of PICs with additional electronic circuits on the other hand. In this context, several research groups have successfully characterized silicon-based PICs, such as couplers, power splitters, optical modulators, wavelength demultiplexers (WDMs) and filters.[3–6] Among them, the structures able to perform wavelength filtering have attracted significant interest mainly due to their potential to be applied not only in telecommunication applications, but also in other fields, such as spectroscopy[7] or sensing.[8]

Different strategies and geometries toward implementing all-optical integrated PICs for filtering have been previously presented. Several types of interference-based integrable spectral filters have been proposed. First are structures that are commonly called single channels, with the most representative being ring resonators[8] and Mach–Zehnder interferometers.[9] Second, a more advanced configuration uses multiple channels or WDMs, in which the current trends are arrayed waveguide gratings[10] and planar concave gratings (also known as echelle gratings).[11] With respect to ring resonators, high Q values are obtained due to the strong field enhancement caused by recursive light propagation inside the structure. This feedback, however, also causes nonlinearities, which distort the device response. Regarding Mach–Zehnder interferometers, the main open issue is related to the critical coupling ratio between the stages, which basically depends on the critical technological steps, as well as the matching between the delay lengths. In the case of WDMs, planar concave gratings have the advantage of a minor footprint; however, in arrayed waveguide gratings, it is possible to selectively tune each delay line and, in general, there is significantly larger design freedom. Nevertheless, in both cases, the required technology is critical, and the robustness against technological variations is very low. The shallow etch configuration[12] partially solves this issue, but at the expense of requiring an additional and highly accurate photolithographic step, and still demands highly precise etching steps. In this context, spectral filtering structures based on both single and multiple channels require an extremely robust technology that uses both critical alignment and etching steps. Nevertheless, they are undoubtedly the workhorse of telecommunication applications. It is also true that such strict technological steps clearly hamper their applications where instead of narrow and sharp peaks, robustness and technological simplicity are key issues. Absorbance-based integrated filters offer an alternative.[13] Typically, their stopband and passband extend to a broad region instead of presenting single/multiple peaks, and absorbance-based integrated filters are easy to implement and characterize. However, the difference between the passband and stopband is not as high when compared

---

[1]Department of Physics, Universitat Autònoma de Barcelona, E-08193 Bellaterra, Barcelona, Spain; [2]Chemical Transducers Group, Institut de Microelectrònica de Barcelona (IMB-CNM, CSIC), E-08193 Bellaterra, Barcelona, Spain and [3]Microsystems Laboratory (LMIS1), École Polytechnique Fédérale de Lausanne (EPFL), CH-1015 Lausanne, Switzerland
Correspondence: R Menchon-Enrich, Department of Physics, Universitat Autònoma de Barcelona, E-08193 Bellaterra, Barcelona, Spain
E-mail: ricard.menchon@uab.cat

Received 26 October 2012; revised 23 January 2013; accepted 28 January 2013

to that of interference filters, and the spectral filtering cannot be tuned because it depends either on the particular organic compound[14] or on the bandgap material in the filter.[15]

In this article, we introduce a completely new method of light spectral filtering, based on the so-called adiabatic passage of light technique.[16–18] We experimentally demonstrate that a system of three identical total internal reflection (TIR) silicon oxide coupled waveguides can act simultaneously as a high- and low-pass spectral filter for the visible range, separating the long and short wavelengths among the different waveguides. We will refer to this type of filter as a spatial adiabatic passage (SAP) filter. The proposed configuration shows a different filtering behavior compared to interference filters,[12] because there is an absence of periodic peaks but a wide transmission band, while maintaining a moderate difference between the passband and stopband values. Moreover, in contrast to absorbance-based filters,[13] the filtering characteristics of the SAP filter can be modified by varying the geometric parameters of the structure. However, variations in a given geometrical parameter value do not imply a severe change in the spectral response. Therefore, in contrast to the interference filters, the SAP filters proposed here have high technological robustness. Additionally, the SAP triple-waveguide system is fully CMOS-compatible and technologically simple to fabricate, requiring only one, non-critical photolithographic step. As such, SAP filters can be monolithically implemented with other electronic elements into photonic integrated circuits with a low-cost and mass-production.

MATERIALS AND METHODS

The propagation of light into a system of three identical single-mode evanescent coupled waveguides can be described through coupled mode equations.[19,20] These equations govern the evolution of the a_i amplitude functions that correspond to the fundamental mode of each i waveguide along the z propagation direction, where $i=L,C,R$ accounts for the left, central and right waveguides, respectively:

$$i\frac{\mathrm{d}}{\mathrm{d}z}\begin{pmatrix} a_R \\ a_C \\ a_L \end{pmatrix} = \begin{pmatrix} 0 & \Omega_R(z,\lambda) & 0 \\ \Omega_R(z,\lambda) & 0 & \Omega_L(z,\lambda) \\ 0 & \Omega_L(z,\lambda) & 0 \end{pmatrix}\begin{pmatrix} a_R \\ a_C \\ a_L \end{pmatrix} \quad (1)$$

where Ω_R (Ω_L) is the coupling coefficient between the central and right (left) waveguides. Because weak coupling is assumed, the right and left waveguides are not directly coupled.

Diagonalizing Equation (1), it can be seen that one of the eigenvectors of the system (supermode) only involves light in the right and left waveguides:

$$D(\Theta) = \begin{pmatrix} \cos\Theta \\ 0 \\ -\sin\Theta \end{pmatrix} \quad (2)$$

with $\tan\Theta \equiv \Omega_R/\Omega_L$. Because the couplings are due to the evanescent fields, they can be easily modified by engineering the transverse waveguide separation along the z propagation direction. In particular, we consider the right waveguide of the SAP filter to be excited by the input light source, and the spatial configuration of the waveguides forces the couplings to follow a counterintuitive sequence along z. Initially, the left waveguide approaches the central waveguide. Later, and with a certain overlap, the right waveguide approaches the central waveguide, whereas the left waveguide separates from the central waveguide, as shown in Figure 1a. With this spatial configuration, the mixing angle, Θ, evolves from 0 to $\pi/2$. If the modification of Θ is adiabatically performed, the supermode (2) is followed, and light

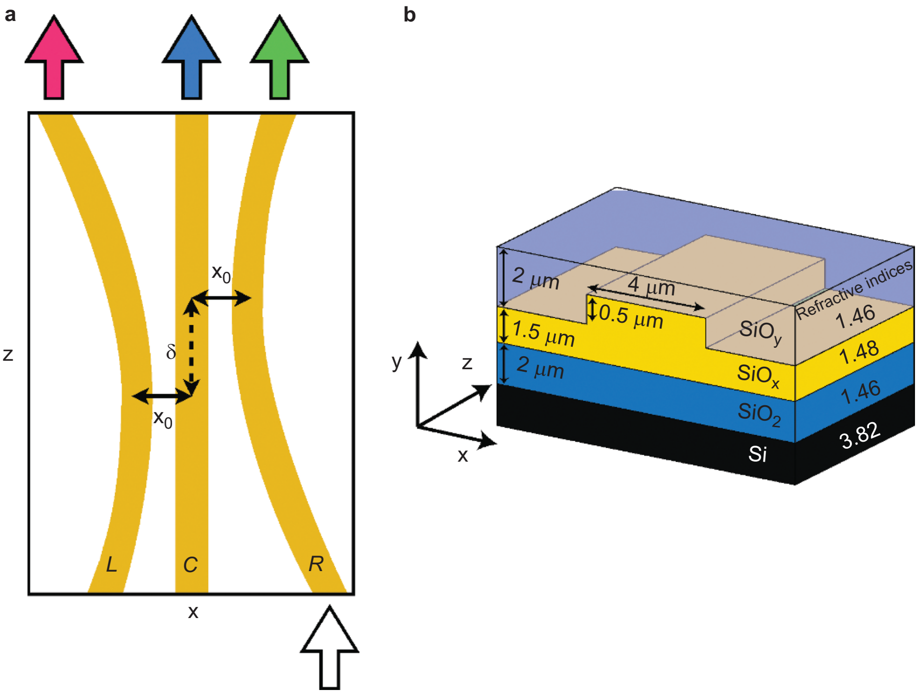

Figure 1 (**a**) A schematic depiction of the SAP filter geometry, viewed from above, consisting of one straight central waveguide (C) and two circularly bent external waveguides, right (R) and left (L). The z separation between the centers of the bent waveguides is given by δ, and the minimum separation between waveguides is defined by x_0. The device's total length in the z direction is $D=2.5$ cm and the external waveguides' radius of curvature is $r=3.5$ m. (**b**) A schematic representation of the different layers of one of the rib waveguides, specifying the refractive indices and materials.

will be efficiently transferred between the outermost waveguides (from right to left in our case) without the propagation of light intensity into the central waveguide.

We also can understand this process by showing the evolution along *z* of the supermodes of the structure.[21,22] In Figure 2, we plot the intensity profile of the supermode (2) from numerical simulations at three different positions along *z* (input, middle and output). The input light into the right waveguide corresponds to the initial spatial distribution of the supermode (2) of the complete structure. Because the geometry of the system is being transformed adiabatically, all of the power remains in the supermode (2), being finally transferred to the left waveguide. As expected from supermode (2), the central waveguide is not involved in the process. This light transfer is the so-called SAP of light,[16–18] which is a very robust and efficient process as long as it is adiabatic. It resembles the stimulated Raman adiabatic passage (STIRAP) technique,[23] which is widely used in quantum optics to transfer atomic or molecular population between the ground levels of a Λ-type three-level system in a robust and highly efficient way. This work represents the first experimental realization of a STIRAP analogous technique, working as a filter. Notice also that in a similar fashion as that in the present work, the SAP technique has been proposed for the robust and efficient transfer of neutral atoms in triple-well traps and waveguides and for the filtering of vibrational matter wave states.[24–26]

Generally, the coupling coefficients between waveguides depend on the wavelength of light, λ, with a dependence that is approximately linear with λ.[19] Considering two identical straight TIR waveguides separated by a distance *d*, the evanescent coupling can be expressed as:

$$\Omega(\lambda,d)=\Omega_0(\lambda)\exp[-d/l(\lambda)] \qquad (3)$$

Numerical simulations[27] of light propagating in a system of two straight waveguides with the parameters indicated in Figure 1b for several separation distances *d* confirm that for a fixed distance *d*, $\Omega(\lambda,d)$ increases linearly with λ for the range of wavelengths of interest in this work (from 400 to 950 nm), as shown in Figure 3a. Additionally, from these simulations, we have obtained the dependence of the decay constant, $l(\lambda)$, on λ, which also grows linearly for the range of working wavelengths.

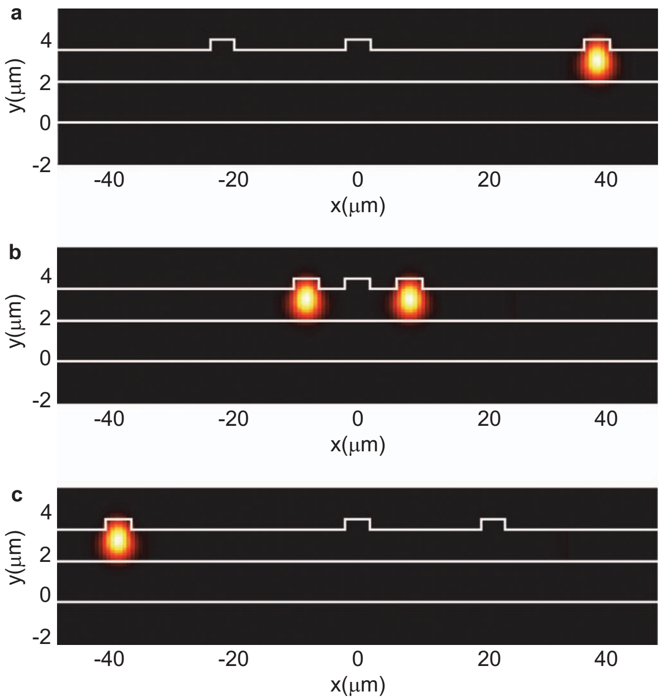

Figure 2 Numerical simulations of the supermode (2) of the triple-waveguide system at three different positions along *z*: (**a**) input, (**b**) middle and (**c**) output. The simulations were calculated with λ=800 nm and the geometrical parameter values of x_0=7 μm and δ=4700 μm.

Using expression (3) for the coupling between each set of two pairs of waveguides in the triple-waveguide system (Figure 1a) and considering the dependence of the separation between waveguides along *z*, we obtain the variation of the couplings along *z*, which follows a Gaussian function:

$$\Omega_{R,L}(z,\lambda)\approx\Omega(\lambda,x_0)\exp\left[\frac{(-z-D/2\pm\delta/2)^2}{2rl(\lambda)}\right] \qquad (4)$$

where δ is the spatial delay between the outermost waveguides, x_0 is the minimum separation between waveguides, *D* is the total length of the system and *r* is the value of the radius of the external waveguides (see Figure 1a). The first factor at the right-hand-side of Equation (4), $\Omega(\lambda,x_0)\equiv\Omega_0(\lambda)\exp[-x_0/l(\lambda)]$, gives the maximum value of the couplings along *z*. It is analogous to expression (3), and therefore, it has the same linear dependence on λ for fixed values of x_0. Moreover, the term, $2rl(\lambda)$, indicates the width of the Gaussian along *z*. Because $l(\lambda)$ grows linearly with λ, the width of the coupling variation along *z* increases as λ increases. In Figure 3b, using the numerically obtained couplings, we represent the spatial dependence of the couplings in the triple-waveguide system for different values of the wavelength. We can observe that the strength and the width of the couplings increase as the wavelength, λ, increases. Note that we have numerically verified that the waveguides used in this work (Figure 1b) are effectively single-mode within the working wavelength range (400–950 nm) and that the coupling rates are polarization independent.

In the SAP filter system composed of three coupled waveguides, light adiabatic passage occurs if the adiabaticity of the light transfer is fulfilled, i.e., if the couplings Ω_R and Ω_L are strong enough, and the overlap between them along the propagation direction *z* is long enough,[16–18,23] as shown in Figure 3b. Thus, for specific values of x_0 and δ of the geometry of the SAP filter, it may be that the couplings are only strong and wide enough along *z* to fulfill the adiabaticity requirements for long enough wavelengths. In this case, longer wavelengths are transferred to the left waveguide. However, for short enough wavelengths, because the couplings are too weak, light is unable to reach the left waveguide, remaining in either the right waveguide or the central waveguide or in a combination of both. Therefore, if we take as the outputs of the SAP filter the left waveguide and the sum of the right and central waveguides, the SAP device simultaneously works as a high-pass and low-pass spectral filter based on the adiabatic passage of light.

We can show more specifically the spectral filtering mechanism in the SAP triple-waveguide system by taking the adjusted parameters of $\Omega(\lambda,x_0)$ and $l(\lambda)$ from the numerical simulations and introducing them into Equation (4) and, finally, integrating Equation (1). The results of the numerical integration for x_0=7 μm and δ=4700 μm are depicted in Figure 4. Figure 4a shows the transmittance at the output of the left, central and right waveguides relative to the total intensity as a function of the wavelength. Although the left waveguide output signal varies smoothly, power oscillations in the right and central waveguide outputs can be observed. Nevertheless, the right and central waveguides could be joined after the device, yielding the result shown in Figure 4b. In this case, the sum of the right and central outputs presents a

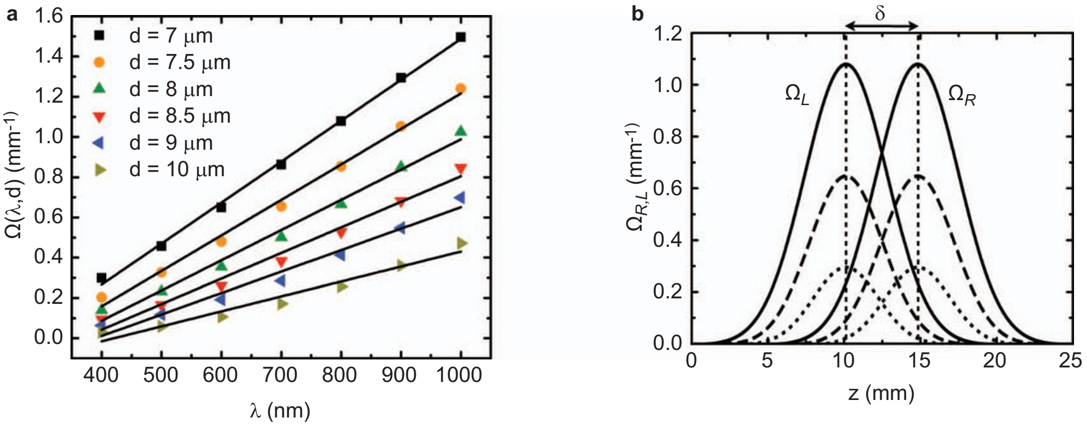

Figure 3 Numerical simulations for the characterization of the couplings. (**a**) The dependence of the coupling coefficient between two straight TIR waveguides (with the characteristics specified in Figure 1b), $\Omega(\lambda,d)$, on λ for fixed distances d. The simulation points are fitted by straight lines. (**b**) The typical counterintuitive sequence of coupling coefficients along z in a system of three coupled waveguides obtained from numerical simulations[27] with x_0=7 μm and δ=4700 μm for different wavelengths, including 400 nm (dotted), 600 nm (dashed) and 800 nm (solid). The increase in the strength and width of the couplings along the z direction can be observed as the wavelength λ increases.

significantly more robust behavior, and we can observe the predicted behavior of the SAP filter which works simultaneously as a high-pass and low-pass spectral filter. In particular, within the range of studied wavelengths, for the left waveguide (high-pass), we find a stopband that reaches a value of −17 dB and a passband of 0 dB. For the sum of the right and central waveguide intensities (low-pass), we find a stopband that reaches −22 dB and a passband of 0 dB. Taking into account that the device can work as a high- and low-pass spectral filter simultaneously, we define the cutoff wavelength, λ_c, as the wavelength for which half of the intensity is at the output of the left waveguide and half at the output of the other two waveguides. Thus, λ_c corresponds to a decrease in intensity of approximately 3 dB and to the point at which the two curves in Figure 4 cross each other. For the presented figure, the cutoff wavelength is 610 nm.

Since SAP filtering is based on the robust technique of the adiabatic passage of light, we expect a similar filtering behaviour, even though the geometric parameter values of the system are significantly modified. Nevertheless, studying the effect of varying the x_0 and δ parameters, we can observe that the specific filtering characteristics of the device (the cutoff wavelength, as well as the stop and passband regions) can be tuned by wavelength. On the one hand, if the spatial delay value δ is increased, the overlap between the couplings becomes smaller. Thus, only strong and wide enough couplings along z will fulfill the adiabaticity condition. On the other hand, if the minimum separation between the waveguides x_0 is increased, the strength of the couplings will be reduced, because the coupling values decay exponentially as the distance between the waveguides increases. Then, stronger and wider couplings (corresponding to long wavelengths) will also be required to maintain the adiabaticity of the process. In conclusion, the filtering characteristics, such as the cutoff wavelength, are moved to longer wavelengths as the values of x_0 and δ increase. The numerical simulations integrating Equation (1) with the adjusted parameters $\Omega(\lambda,x_0)$ and $l(\lambda)$ support this reasoning, as it can be observed in Figure 5.

Numerical simulations were performed to optimize the geometry of the triple-waveguide SAP filter for different wavelengths[27] such that the obtained parameter values were used to define the required technological steps. The SAP filters were fabricated with a total length of

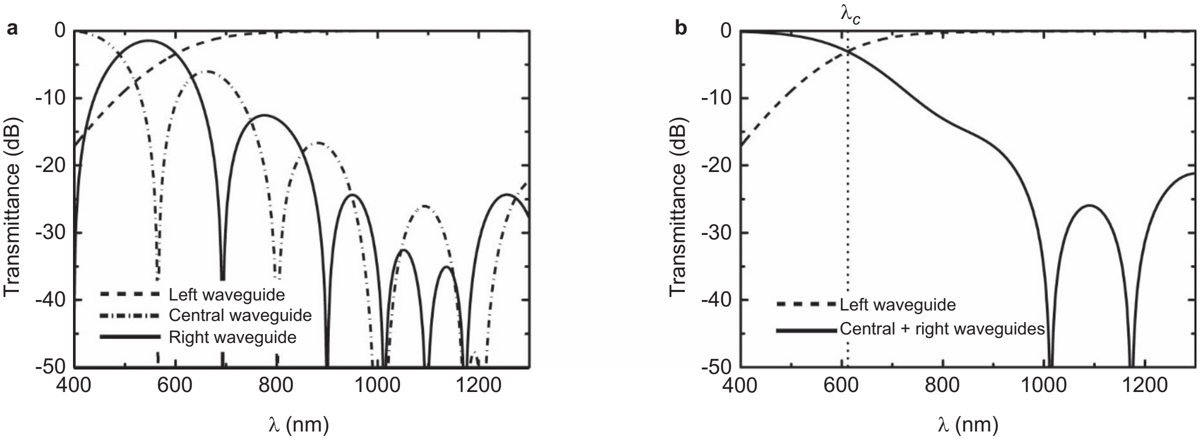

Figure 4 The results of the numerical integration of Equation (1) with parameter values x_0=7 μm and δ=4700 μm. (**a**) The transmittance at the output of the left (dashed line), central (dashed-dotted line) and right (solid line) waveguides, represented relative to the total output intensity as a function of the wavelength. In (**b**), the high- and low-pass filtering behavior for a SAP filter can be observed, represented as the transmittance at the output of the left (dashed line) and the sum of the central and the right (solid line) waveguides relative to the total output intensity with respect to the wavelength. No losses are considered when integrating Equation (1).

2.5 cm, and external waveguides were given a radius of curvature of 3.5 m. To obtain devices with different filtering characteristics, for every system of waveguides, slightly different parameter values of the spatial delay δ and minimum separation between waveguides x_0 also were fabricated.

The fabrication process for the triple-waveguide systems includes the following stages. Initially, a 2-μm-thick layer of SiO_2 was thermally grown on a (100) silicon wafer. After that, a layer of non-stoichiometric silicon oxide SiO_x with a refractive index of 1.48 and a height of 2 μm was deposited by plasma-enhanced chemical vapor deposition.[28] At this stage, ribs of 4 μm width and a thickness of 0.5 μm in the SiO_x layer were defined by using the previously designed mask and dry etching, and the waveguides were obtained. Finally, a 2-μm-thick passivation layer of non-stoichiometric silicon oxide SiO_y with refractive index 1.46 was deposited using plasma-enhanced chemical vapor deposition. Figure 1b shows the transverse profile of a waveguide belonging to the triple-waveguide system, specifying the sizes of the layers and the refractive index values, which were measured by ellipsometry.[28]

The experimental setup is composed of a halogen white light source (Ocean Optics HL-2000-HP-FHSA, Dunedin, Florida, USA) connected to a 4-μm core optical fiber (Thorlabs 600HP, Newton, New Jersey, USA). The position of the other end of the fiber is controlled by a piezoelectric three-dimensional positioning system (Piezosystem Jena NV40/3, Jena, Germany), which provides nanometer-scale precision alignment between the optical fiber and the waveguide. The light emerging from the system is collected by another 4-μm core optical fiber, placed on another piezoelectric positioning system (Piezosystem Jena d-Drive) and transmitted to a microspectrometer (Ocean Optics QE65000).

With respect to the losses of the SAP filter, since the final goal of our proposal is to place the device into a PIC, we are mainly interested in the losses produced by the SAP geometry of the system, i.e., those losses due to the couplings and the bending of the waveguides, but not in the insertion and propagation losses, which depend on the characteristics of the specific waveguides. Thus, we studied the losses due to the adiabatic passage geometry by comparing the sum of the output intensities of the three waveguides of the device with the output of a single straight waveguide with equal features and the same length as the system of three waveguides. The experimental and numerical tests show that the losses due to the adiabatic passage geometry are negligible. With respect to the range of wavelengths available in the presented experimental setup, 400–950 nm can be sampled. The range is mainly limited by the allowed wavelengths propagating inside the fibers in addition to the sensitivity of the microspectrometer.

RESULTS AND DISCUSSION

The result shown in Figure 6 experimentally demonstrates the spectral filtering, based on the adiabatic passage of light technique for one of the fabricated SAP filters with a minimum separation between waveguides of $x_0=9$ μm and a spatial delay of $\delta=5200$ μm. Figure 6a shows the intensity at the output of the left, central and right waveguides as transmittance relative to the total output intensity (we previously verified that the losses due to the adiabatic passage geometry are negligible). As expected from the numerical simulations, some power oscillations can be observed between the right and central waveguides, depending on the wavelength. However, we could join the right and central waveguides in a single waveguide just after the described triple-waveguide system by appropriately designing the photomask used for fabrication. By doing this, we would obtain an output corresponding to the sum of the right and central waveguides, which presents a significantly smoother and more robust behavior, as obtained from the numerical simulations. Thus, Figure 6b represents the experimentally measured intensity at the output of the left waveguide and the sum of the outputs of the right and central waveguides as the transmittance relative to the total output intensity.

From this result, we experimentally conclude that the triple-waveguide SAP filter acts as a high-pass (output at the left waveguide) and low-pass (output at the central and right waveguides) spectral filter, representing a new and different filtering behavior in comparison to interference filters[12] and absorbance-based filters.[13] We have obtained a filtering efficiency between the efficiency of the inteference and the absorbance-based filters. In particular, the measured values for the left waveguide output (high-pass) reach a value of approximately −11 dB for the stopband, and the passband is close to 0 dB. For the sum of right and central (low-pass) waveguides, the stopband is approximately −20 dB and the passband −0.5 dB. The measured cutoff wavelength is 638 nm.

As discussed in the 'Materials and methods' section, SAP filters allow for a modification of the filtering characteristics (the cutoff

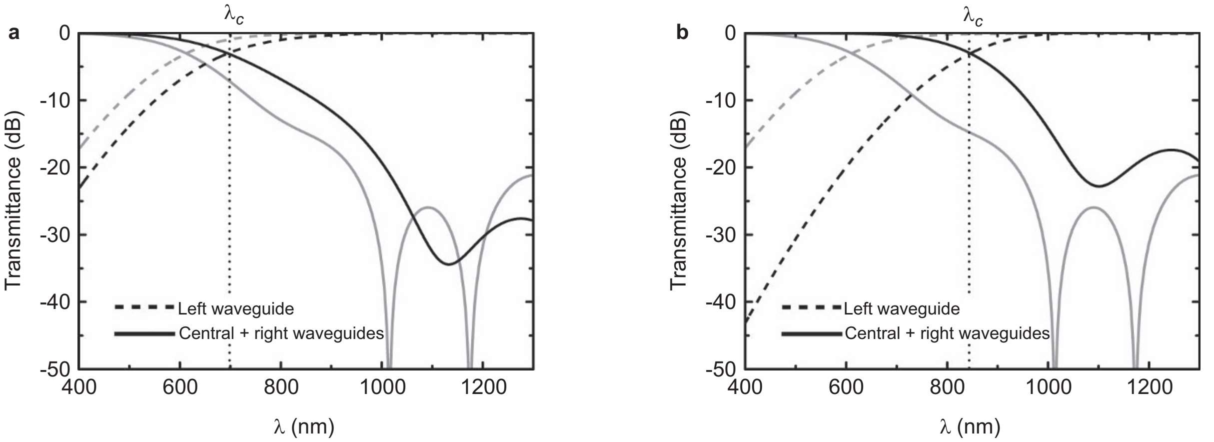

Figure 5 The numerical simulations of the high- and low-pass spectral filtering behavior for a SAP filter with (**a**) $x_0=7$ μm and $\delta=5700$ μm and (**b**) $x_0=9$ μm and $\delta=4700$ μm. In comparison with the curves in Figure 4 with $x_0=7$ μm and $\delta=4700$ μm (light grey in these figures), we observe that when increasing the value of (**a**) δ and (**b**) x_0, the cutoff wavelength of the device is moved to longer wavelengths. In all cases, the output of the left (central and right) waveguides corresponds to the dashed (solid) line.

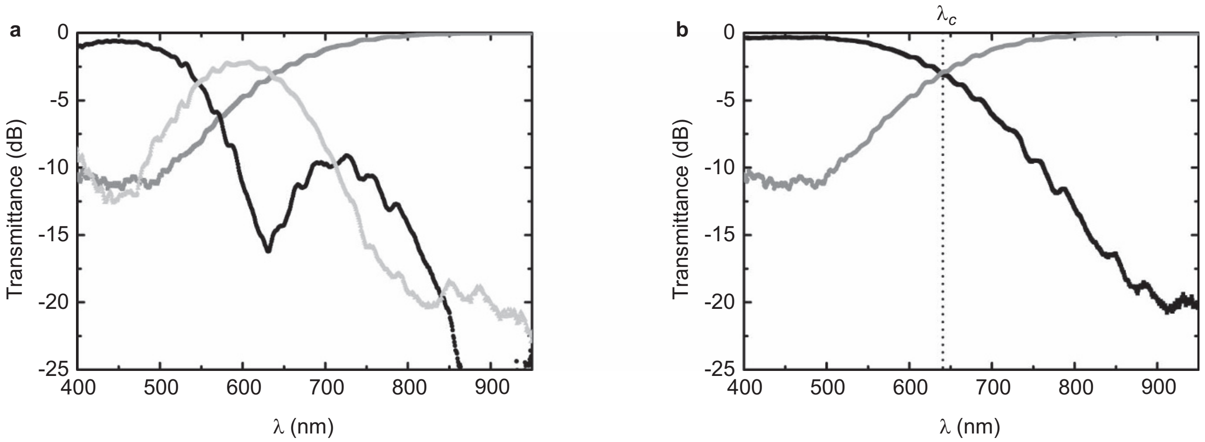

Figure 6 (**a**) The measured intensity, represented as transmittance at the left (grey), central (black) and right (light grey) outputs relative to the total output intensity as a function of the wavelength. (**b**) The measured intensity, represented as transmittance at the left (grey) and the sum of the central and the right (black) outputs relative to the total output intensity with respect to the wavelength. The parameter values for this specific device are x_0=9 μm and δ=5200 μm. The experimental cutoff wavelength in this case is λ_c=638 nm.

wavelength, stopband and passband) by changing the parameter values δ and x_0. Figure 7 shows the measured transmittance of various systems with different δ parameter values (3700, 4200, 4700, 5200 and 5700 μm) for different x_0 values (7, 7.5, 8 and 9 μm). Within the measurement range (400–950 nm), similar slopes, values of the stopband at approximately −20 dB for the sum of the right and central waveguides and values up to −12 dB for the left waveguide can be observed, which are expected to be lower for shorter wavelengths (not available with our setup). The values of the passband are very close to 0 dB for both cases whenever the value is within the measurement range. In Figure 7, we also observe some oscillations of the transmittance for the sum of the central and right outputs, which supports the numerical analysis previously described, as shown in Figures 4 and 5. These oscillations do not affect the high- and low-pass filtering behavior of the SAP filter. Furthermore, as already anticipated, for a fixed value of x_0, the transmittance curves are shifted to longer wavelengths for an increasing value of the δ parameter. Similarly, for a fixed value of δ, increasing the value of x_0 also shifts the transmittance curves to longer wavelengths. This change in the filtering characteristics represents an improvement in comparison to absorbance-based filters. Moreover, it can be observed that in contrast to interference filters, varying some of the geometric parameter values of the SAP filters does not imply that there is a drastic modification of the spectral response of the SAP filter.

Figure 8 shows the evolution of the cutoff wavelength when varying the δ and x_0 parameter values. It can clearly be observed that the cutoff wavelength increases as δ and x_0 increase. Furthermore, Figure 8 could be used to adjust the numerical simulations to the experimental results to obtain the value of the real couplings acting in the fabricated devices.

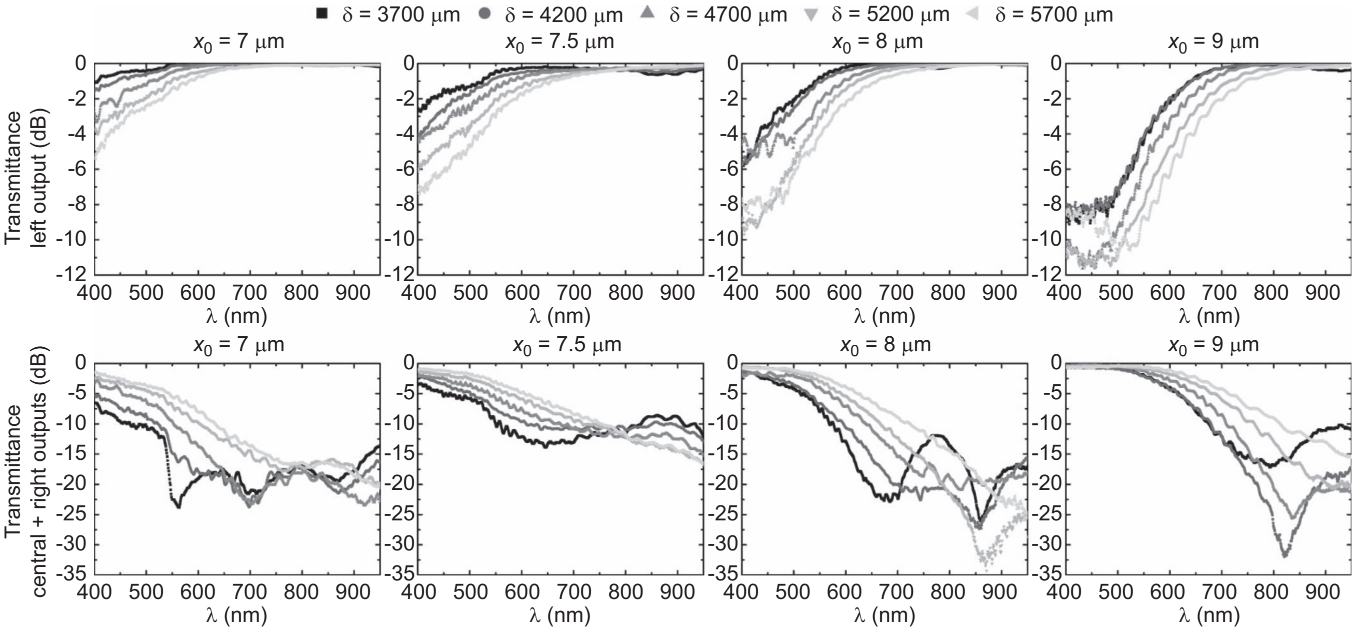

Figure 7 The experimental measurements of the left (upper row) and the sum of the central and right (lower row) output transmittance for different values of δ and x_0.

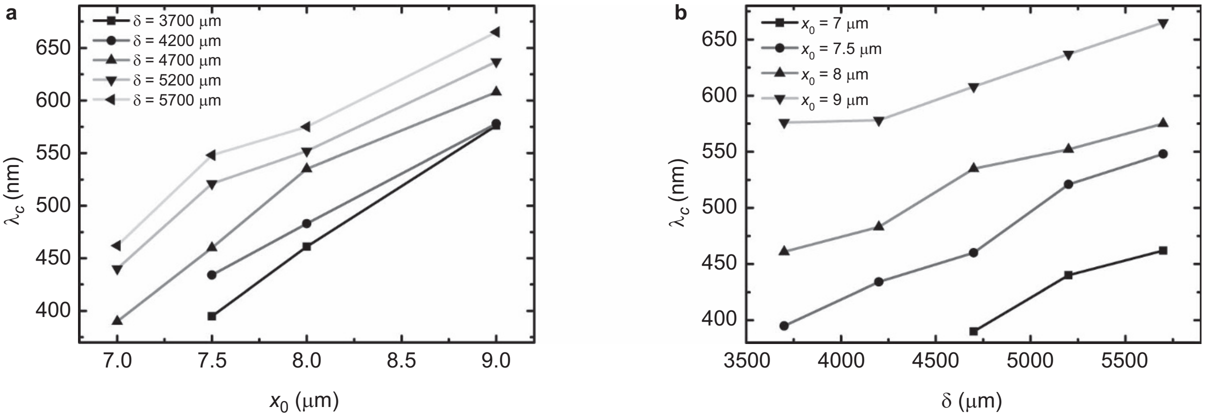

Figure 8 The variation in the cutoff wavelength as a function of (**a**) x_0 for different values of δ and (**b**) δ for different values of x_0.

If we compare the experimental figures (Figures 6 and 7) with the numerical figures (Figures 4 and 5), the qualitative filtering behavior is the same, although some differences arise. The first is that the stopbands obtained through numerical simulations reach deeper values than the experimental stopbands. It can be observed that for some cases, the measured values of the intensity at extreme values of the considered range of wavelengths tend to stabilize; however, in the numerical simulations, the values continue evolving to lower transmittance values. This difference can be explained because at the limits of both short and long wavelengths, the efficiency of the microspectrometer used is very low. Therefore, the signal-to-noise ratio is very small. Additionally, the maximum dynamic range available with our setup is 35 dB, and consequently, the stopband values that can be measured are limited to this value. Nevertheless, such a value is sufficient to confirm the validity of the configuration proposed here. Second, it can be observed that for the experimental case, the filtering behavior is shifted to shorter wavelengths in comparison to the numerical curves, which may be associated with a slight variation in the thicknesses and/or refractive indices of the layers in the fabrication process. However, this result does not affect the overall behavior of the proposed device. Additionally, the result confirms the device's robustness against technological variations and validates these SAP filters as efficient and cost-effective integrable devices.

CONCLUSIONS

We have theoretically and experimentally demonstrated that it is possible to use a triple-waveguide system, with identical coupled TIR silicon oxide waveguides, as a simultaneous high- and low-pass spectral filter, based on the SAP of light technique. Light is injected into the right waveguide of the system, and after propagating along the system, long wavelengths are transferred into the left output; in contrast, short wavelengths propagate to the central and right outputs. We refer to this device as the SAP filter, which constitutes the first experimental realization of an analogous of the STIRAP technique working as a filter. The SAP filter represents an alternative to other integrated filtering devices, such as interference filters or absorbance-based filters. Additionally, since the waveguides used in the fabricated SAP filters are fully CMOS-compatible, they could be monolithically integrated with other photonic and electronic elements into a photonic integrated circuit, allowing low cost and mass production.

We also demonstrated that upon varying the minimum distance between waveguides, x_0, and the spatial delay between the external waveguides, δ, the filtering characteristics of the system can be modified. In particular, we have shown that if the values of x_0 or δ are increased, the cutoff wavelength, which separates the low- and high-pass filtering regions, is shifted to longer wavelengths. In this way, by modifying the fabrication parameter values, it is possible to adapt the filtering characteristics of the device to fit specific requirements. However, these variations do not change the general filtering behavior of the SAP filter, which confirms its robustness with respect to technological variations.

Although we have focused this work within the visible range, an extension to infrared wavelengths is straightforward and would allow future implementation of this SAP filter into the standard frequency range of telecommunications.

ACKNOWLEDGMENTS

This work was supported by the Spanish Ministerio de Ciencia e Innovación under contracts FIS2008-02425, FIS2011-23719 and CSD2006-0019 and by the Catalan Government under contract SGR2009-00347. R Menchon-Enrich acknowledges the support received from the Spanish Ministerio de Educación under grant AP2008-01276. Funding from the European Research Council under the European Community's Seventh Framework Programme (FP7/2007-2013)/ERC grant agreement number 209243 is also acknowledged.

---

1 Baets R, Dumon P, Bogaerts W, Roelkens R, van Campenhout J *et al.* Silicon Photonics. International Symposium on VLSI Technology, Systems and Applications, 2007. *VLSI-TSA* 2007; 1–3; 23 Apr-25 Apr 2007, Hsinchu, Taiwan.
2 Bogaerts W, Dumon P, Luyssaert B, Bienstman P. Nanophotonic waveguides in silicon-on-insulator fabricated with CMOS technology. *J Light Tech* 2005; **23**: 401–412.
3 Llobera A, Salinas I, Garcés I, Merlos A, Domínguez C. Effect of the wall tilt on the optical properties of integrated directional couplers. *Opt Lett* 2002; **27**: 601–603.
4 Barrios CA, Sanchez B, Gylfason KB, Griol A, Sohlstrom H *et al.* Demonstration of slot-waveguide structures on silicon nitride/silicon oxide platform. *Opt Express* 2007; **15**: 6846–6856.
5 Sahu PP. A tapered structure for compact multimode interference coupler. *IEEE Photon Technol Lett* 2008; **20**: 638–640.
6 Miller DAB. Device requirements for optical interconnects to silicon chips. *Proc IEEE* 2009; **97**: 1166–1185.
7 Yang WG, Conkey DB, Wu B, Yin D, Hawkins AR *et al.* Atomic spectroscopy on a chip. *Nat Photon* 2007; **1**: 331–335.
8 de Vos K, Bartolozzi I, Schacht E, Bienstman P, Baets R. Silicon-on-insulator microring resonator for sensitive and label-free biosensing. *Opt Express* 2007; **15**: 7610–7615.
9 Prieto F, Sepúlveda B, Calle A, Llobera A, Domínguez C *et al.* An integrated optical interferometric nanodevice based on silicon technology for biosensor applications. *Nanotechnology* 2003; **14**: 907–912.
10 Bogaerts W, Dumon P, van Thourhout D, Taillaert D, Jaenen P *et al.* Compact wavelength-selective functions in silicon-on-insulator photonic wires. *IEEE J Sel Top Quantum Electron* 2006; **12**: 1394–1401.

11 Brouckaert J, Bogaerts W, Dumon P, van Thourhout D, Baets R. Planar concave grating demultiplexer fabricated on a nanophotonic silicon-on-insulator platform. *J Lightw Technol* 2007; **25**: 1269–1275.

12 Bogaerts W, Selvaraja SK, Dumon P, Brouckaert J, de Vos K *et al*. Silicon-on-insulator spectral filters fabricated with CMOS technology. *IEEE J Sel Top Quantum Electron* 2010; **16**: 33–44.

13 Llobera A, Demming S, Joensson HN, Vila-Planas J, Andersson-Svahn H *et al*. Monolithic PDMS passband filters for fluorescence detection. *Lab Chip* 2010; **10**: 1987–1992.

14 Chabinyc ML, Chiu DT, McDonald JC, Stroock AD, Christian JF *et al*. An integrated fluorescence detection system in poly(dimethylsiloxane) for microfluidic applications. *Anal Chem* 2001; **73**: 4491–4498.

15 Mahan AH, Biswas R, Gedvilas LM, Williamson DL, Pan BC. On the influence of short and medium range order on the material band gap in hydrogenated amorphous silicon. *J Appl Phys* 2004; **96**: 3818–3826.

16 Longhi S, Della Valle G, Ornigotti M, Laporta P. Coherent tunneling by adiabatic passage in an optical waveguide system. *Phys Rev B* 2007; **76**: 201101.

17 Lahini Y, Pozzi F, Sorel M, Morandotti R, Christodoulides DN *et al*. Effect of nonlinearity on adiabatic evolution of light. *Phys Rev Lett* 2008; **101**: 193901.

18 Menchon-Enrich R, Llobera A, Cadarso VJ, Mompart J, Ahufinger V. Adiabatic passage of light in CMOS-compatible silicon oxide integrated rib waveguides. *IEEE Photon Technol Lett* 2012; **24**: 536–538.

19 Chen CL. Foundations for Guided-Wave Optics. New Jersey: John Wiley & Sons; 2007.

20 Okamoto K. Fundamentals of Optical Waveguides. Burlington, MA: Elsevier; 2006.

21 Sun X, Liu HC, Yariv A. Adiabaticity criterion and the shortest adiabatic mode transformer in a coupled-waveguide system. *Opt Lett* 2009; **34**: 280–282.

22 Galarza M, van Thourhout D, Baets R, Lopez-Amo M. Compact and highly-efficient polarization independent vertical resonant couplers for active-passive monolithic integration. *Opt Express* 2008; **16**: 8350–8358.

23 Bergmann K, Theuer H, Shore BW. Coherent population transfer among quantum states of atoms and molecules. *Rev Mod Phys* 1998; **70**: 1003–1025.

24 Eckert K, Lewenstein M, Corbalán R, Birkl G, Ertmer W *et al*. Three-level atom optics *via* the tunneling interaction. *Phys Rev A* 2004; **70**: 023606.

25 Eckert K, Mompart J, Corbalán R, Lewenstein M, Birkl G. Three level atom optics in dipole traps and waveguides. *Opt Commun* 2006; **264**: 264–270.

26 Loiko Yu, Ahufinger V, Corbalán R, Birkl G, Mompart J. Filtering of matter-wave vibrational states *via* spatial adiabatic passage. *Phys Rev A* 2011; **83**: 033629.

27 Fimmprop and Fimmwave (Photon Desing, Oxford, UK) have been used to perform the numerical simulations.

28 Domínguez C, Rodríguez JA, Riera M, Llobera A, Díaz B. Effect of hydrogen-related impurities on the thermal behaviour of mechanical stress in silicon oxides suitable for integrated optics. *J Appl Phys* 2003; **93**: 5125–5130.